

Investigating the hemodynamics of Berlin Heart EXCOR support in Norwood patients across diverse clinical scenarios with computational modeling

Victoria Yuan¹  | Francesco De Gaetano²  | Kasra Osouli² | Alison L. Marsden³ | Maria Laura Costantino² 

¹David Geffen School of Medicine at UCLA, Los Angeles, California, USA

²Chemistry, Materials and Chemical Engineering Department “Giulio Natta”, Politecnico di Milano, Milan, Italy

³Department of Pediatrics and Bioengineering, Stanford University, Stanford, California, USA

Correspondence

Victoria Yuan, David Geffen School of Medicine at UCLA, Los Angeles, CA, USA.

Email: vyuan@mednet.ucla.edu

Funding information

Fulbright Association

Abstract

Background: Infants with single-ventricle (SV) physiology undergo the 3-stage Fontan surgery. Norwood patients, who have completed the first stage, face the highest interstage mortality. The Berlin Heart EXCOR (BH), a pediatric pulsatile ventricular assist device, has shown promise in supporting these patients. However, clinical questions regarding device configurations prevent optimal support.

Methods: We developed a combined idealized mechanics-lumped parameter model of a Norwood patient and simulated two additional patient-specific cases: pulmonary hypertension (PH) and post-operative treatment with milrinone. We quantified the effects of BH support across different device volumes, rates, and inflow connections on patient hemodynamics and BH performance.

Results: Increasing device volume and rate increased cardiac output, but with unsubstantial changes in specific arterial oxygen content. We identified distinct SV–BH interactions that may impact patient myocardial health and contribute to poor clinical outcomes. Our results suggested BH settings for patients with PH and for patients treated post-operatively with milrinone.

Conclusions: We present a computational model to characterize and quantify patient hemodynamics and BH support for infants with Norwood physiology. Our results emphasized that oxygen delivery does not increase with BH rate or volume, which may not meet patient needs and contribute to suboptimal clinical outcomes. Our findings demonstrated that an atrial BH may provide optimal cardiac loading for patients with diastolic dysfunction. Meanwhile, a ventricular BH decreased active stress in the myocardium and countered the effects of milrinone. Patients with PH showed greater sensitivity to device volume. In this work, we demonstrate the adaptability of our model to analyze BH support across varied clinical situations.

KEYWORDS

Berlin Heart EXCOR, lumped parameter model, Norwood palliation, pulsatile ventricular assist device, single-ventricle physiology

This is an open access article under the terms of the [Creative Commons Attribution-NonCommercial-NoDerivs](https://creativecommons.org/licenses/by-nc-nd/4.0/) License, which permits use and distribution in any medium, provided the original work is properly cited, the use is non-commercial and no modifications or adaptations are made.

© 2023 The Authors. *Artificial Organs* published by International Center for Artificial Organ and Transplantation (ICAOT) and Wiley Periodicals LLC.

1 | INTRODUCTION

Infants with single-ventricle (SV) physiology undergo the Fontan palliation, which consists of the Norwood, Glenn, and Fontan operations. This three-stage surgery separates the pulmonary and systemic circulations by re-routing the venous circulation to pass through the lungs without entering a ventricle. The Norwood procedure occurs when the patient is a few days old, and a 3–4 mm systemic-to-pulmonary shunt is created to act as the only source of pulmonary blood flow. However, these infants are the most vulnerable during the Fontan palliation and face an interstage mortality of 23%.¹ SV patients have benefited from support with the Berlin Heart EXCOR (BH). The BH is a pulsatile, extracorporeal ventricular assist device (VAD) that has successfully bridged 75%–92% of all implanted patients to transplant.² The device consists of an air chamber and blood chamber, separated by a thin, flexible membrane. High pressure in the air chamber displaces the membrane, which in turn pushes output to the native circulation. The inflow tubing for the BH blood chamber can be connected at the atrium or ventricular apex, with outflow at the ascending aorta.³ The BH comes in volumes from 10 to 60 mL, and clinicians can modulate four settings: device rate, systolic time, and systolic and diastolic drive pressures to ensure sufficient device output.

However, outcomes for Norwood patients on the BH are significantly worse than their biventricular counterparts.⁴ In a multi-center study, Weinstein et al. reports that SV patients face a success rate of 42.3%, compared with 72.5% for biventricular patients.⁴ Among these SV patients, only 11.1% neonates with Norwood palliation were successfully supported, compared with 58.3% of Glenn and 60% of Fontan patients. The lower body surface area of Norwood patients does not thoroughly explain their outcomes.⁴ Rather, clinicians cite difficulties in determining the appropriate BH volume, rate, and inflow placement at the atrium versus ventricle.^{3,5} Outcomes for Norwood patients are also impacted by risk factors such as pulmonary hypertension (PH), which is associated with heart failure and mortality.^{3,5–7}

The impact of the Berlin Heart on the Norwood patient physiology has not been widely studied. Clinical experiences are limited to single-center reports, whereas prior *in vitro* studies of the Norwood physiology have not included VAD implantation.^{8–10} Computational modeling offers an avenue to investigate the hemodynamics of the Norwood physiology and its relationship to patient outcomes.^{11–15} However, prior *in silico* studies focused primarily on continuous flow devices in children with the Fontan physiology, whereas pulsatile VADs are more commonly used in Norwood patients.^{4,8–10,16–20} Given the complex physiologies of Norwood patients and limited clinical experiences,

computational simulations can help paint a fuller picture of the hemodynamics of different BH configurations and inform decision-making on patient-specific treatments.

In this work, we leveraged a clinically validated model of the Norwood physiology and BH to characterize how device inflow connection, volume, and rate impact patient hemodynamics and device performance.^{11,21} We then simulated a child with PH and investigated device support in this physiology. Finally, we explored the combined impact of VAD support and post-operative pharmacologies by modeling milrinone infusion together with BH implantation. To the best of our knowledge, we present the first computational study of a pulsatile VAD in a Norwood infant which explores diverse clinical scenarios.

2 | METHODS

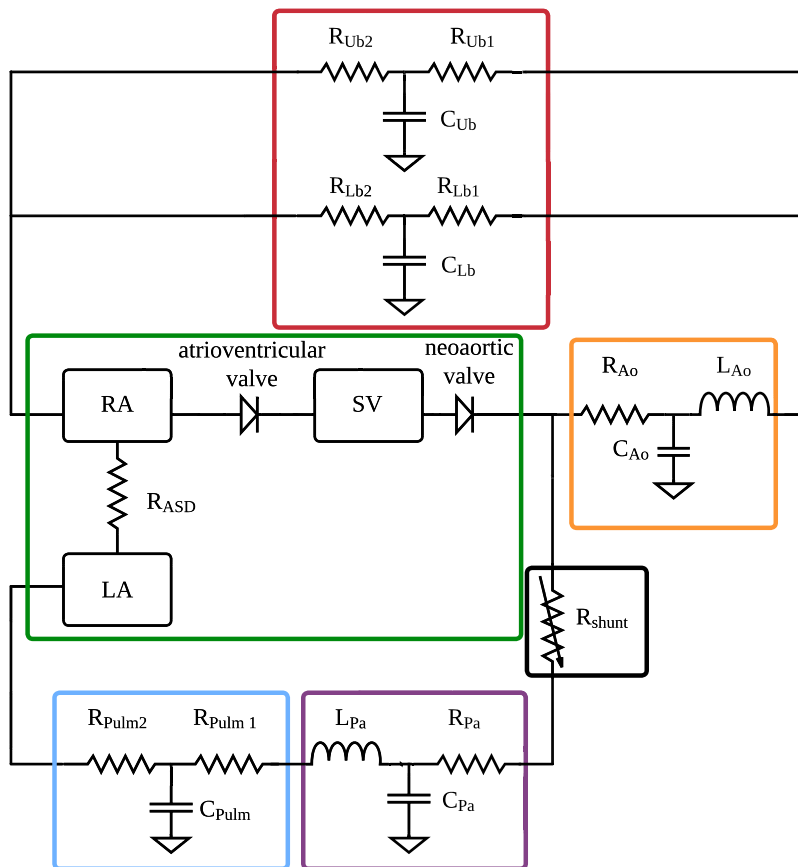
We developed a combined idealized mechanics-lumped parameter model of the Norwood physiology by adapting previously developed models.^{11,22} The BH was represented by an existing lumped parameter model based on idealized device mechanics.²¹ Simulations were performed over 24 cardiac cycles (12s). For a heart rate of 120 beats per minute and a BH rate of 85 pumps per minute, this corresponds to the minimum time for an integer number of BH pumps and allows full exploration of SV–BH phase interactions. The initial state was SV systole. Our model converged after six cardiac cycles (3s). Cardiac output (CO), ventricular stroke work (VSW), specific arterial oxygen content (SpO₂), and other clinically relevant metrics were calculated after convergence to assess patient hemodynamics, physiologic changes, and device performance.

2.1 | Model of Norwood physiology

Using clinical measurements of a cohort of Norwood patients, we represented a 3-month-old infant with Norwood physiology and a BSA of 0.33 m² (Figure 1).^{11,13} Our model consisted of six components:

1. The atria and SV were represented using the 1D single-fiber cardiac model to capture the relationship between myocardial mechanics and organ-level behavior.²² The parameters governing myocardial behavior were tuned to clinically reported end-systolic and end-diastolic volumes.¹¹
2. A non-obstructive atrial septal defect (ASD) was modeled as a resistor connecting the left and right atria.¹¹
3. The inflow and outflow valves of the SV are represented using the simplified valve model from Mynard et al., where the valve state δ depended on instantaneous

FIGURE 1 Lumped parameter model of an infant with Norwood physiology with the heart outlined in green, the aorta in orange, the systemic circulation in red, the systemic-to-pulmonary shunt in black, the pulmonary artery in purple, and the distal pulmonary circulation in blue.



pressure differences.²³ We define δ , ($0 \leq \delta \leq 1$), such that $\delta = 0$ was a closed valve and $\delta = 1$ was open.

4. The systemic circulation was represented with the aorta as a resistor-inductor-capacitor (RLC) circuit, the upper body circulation as a resistor-capacitor-resistor (RCR) circuit, and the lower body circulation as an RCR circuit. We obtained systemic vascular resistance (SVR) and inductance from clinical measurements.¹¹ Aortic resistance was 5% of total SVR. We assumed equal resistive and capacitive values for the upper and lower body to capture neonatal physiology.¹¹
5. The pulmonary circulation was modeled with the pulmonary artery (PA) as an RLC circuit and the distal circulation as an RCR circuit. We obtained pulmonary vascular resistance (PVR) and inductance from clinical measurements; resistance of the PA was 5% of PVR, and distal resistance was 95%.¹¹ To simulate pulmonary hypertension (PH), we doubled PVR to match clinically measured values and distributed resistances as described.³²
6. A nonlinear element represented the Blalock–Taussig shunt with a diameter of 3.5 mm, such that the pressure drop ΔP across the shunt was¹¹:

$$\Delta P = \frac{k_1}{D^4} Q(t) + \frac{k_2}{D^4} Q(t)^2, \quad (1)$$

where k_1 and k_2 are proportionality constants, D is the shunt diameter, and $Q(t)$ is the instantaneous flow across the shunt.

To reflect the typical physiology of a Norwood patient, indexed systemic vascular resistance (SVR_i) and indexed pulmonary vascular resistance (PVR_i) were set to 21 Wood units \cdot m² and 3.5 Wood units \cdot m², respectively, and heart rate (HR) to 120 beats per minute (bpm).¹³

2.1.1 | Simulating post-operative management with milrinone

Milrinone is a positive inotrope, vasodilator, and common post-operative treatment in Norwood patients.^{24–27} We combined data from clinical and experimental studies to simulate post-operative milrinone infusion in Norwood patients. In a cohort of neonates with congenital heart disease, clinical reports measured a 3% increase in HR and a 37.5% and 27.2% decrease in SVR and PVR, respectively.²⁸

We then leveraged experimental data from Gao et al., to quantify changes in myocardial dynamics as a function of μ M of milrinone. Given clinically measured concentrations of 4.28 μ M of milrinone in Norwood patients after 24 h, we tuned our single-fiber model of the SV to capture increases of 5% in the amplitude of sarcomere shortening, 50% in the maximum systolic shortening velocity, and 20% in the maximum diastolic shortening velocity.²⁹



2.2 | Model of the Berlin Heart

Using a previously developed model in Yuan et al., we simulated the BH in three parts²¹:

1. The inflow and outflow tubing were modeled as Poiseuille resistors. Length and diameter were taken from the instructions for use as outlined by the Berlin Heart GmbH.³⁰
2. The inflow and outflow valves of the BH were represented using the valve model from Mynard et al. described in Section 2.1.
3. The air and blood chambers were modeled as an idealized sphere divided by a thin, massless plate that is clamped along the edges. The displacement ω is measured from center plane to peak deflection. We assumed linear membrane deformations given a uniformly distributed pressure load. Displacement of the membrane varied as a function of the pressure difference between the air and blood chambers. Based on classical results for linear, elastic, clamped, circular membranes, the following equation governs membrane dynamics:

$$\frac{\partial}{\partial r} \left[\frac{1}{r} \frac{\partial}{\partial r} \left(r \frac{\partial \omega}{\partial r} \right) \right] = \frac{(P_a - p_{in})r}{2D}, \quad (2)$$

where r is the radial coordinate from the membrane center, ω is displacement of the membrane, P_a is the prescribed air chamber pressure, p_{in} is the pressure in the BH blood chamber, and D is the stiffness parameter of the membrane. The resulting solution is:

$$\omega(r) = \omega_{\max} \left(1 - \frac{r^2}{R^2} \right)^2, \quad (3)$$

such that

$$\omega_{\max} = \frac{[P_a - p_{in}]R^4}{64D}, D = \frac{Eh^3}{12(1 - \mu^2)}, \quad (4)$$

where ω_{\max} is the maximum displacement, P_a is the air chamber pressure, p_{in} is the pressure in the BH blood chamber, R is the radius of the BH, E is Young's modulus, h is membrane thickness, and μ is Poisson's ratio. By integrating Equation (3), the volume displaced by the BH membrane can be calculated as:

$$V_{\text{displaced}} = \frac{1}{3} \pi R^2 \omega_{\max}. \quad (5)$$

We assume equivalent terminal pressures within the device and apply conservation of blood volume to complete the model.

2.3 | Modeling BH implantation

We studied the relationship between patient hemodynamics, BH performance, and three different device parameters—inflow connection, volume, and rate. BH inflow was connected at either the atrium or ventricular apex, with outflow at the ascending aorta. Volumes of 10, 15, and 25 mL were simulated as they are recommended for the corresponding age and BSA of Norwood patients.³⁰ The device was driven at 220/−30 mm Hg and 85 pumps per minute (ppm) to represent average operating conditions.⁴ To study device rate, we simulated a 10 mL BH at rates of [60, 120] ppm, inclusive, at intervals of 10 ppm. The device was driven at 220/−30 mm Hg.

As the BH ejection is not synchronous with SV systole, we captured SV–BH interactions in all simulations by shifting the phase of BH ejection relative to SV systole by $[-\pi, \pi]$ at intervals of $\frac{\pi}{4}$. Given previous work on modeling the BH, phase shifts of $\frac{\pi}{4}$ were simulated to save computational cost as, upon initial quantitative analysis, there was no significant difference between simulation results for $\frac{\pi}{8}$ and $\frac{\pi}{4}$.²¹

Results for each device configuration were then averaged over time and phase. For each HR–device rate combination, we simulated nine phases, with results from each phase averaged over 9 s of simulation. Thus, for each HR–device rate combination, 81 s were simulated. CO, VSW, oxygen delivery, and other hemodynamic variables were quantified. We define BH efficiency as volumetric efficiency, which is the observed output divided by the theoretical output, which in turn is the product of device rate and volume. We repeated these studies on device volume, rate, and connection for a Norwood patient with PH and a patient treated post-operatively with milrinone.

3 | RESULTS

Simulation results are outlined in three subsections. Each subsection is stratified by patient physiology. We analyze the impact of varying device volume and rate and comparisons between atrial versus ventricular inflow connections are drawn. We also quantify myocardial active stress, which we define as the stress in the myocardium at end-systole, and passive stress, the stress in the myocardium at end-diastole. Hemodynamic results for the Norwood patient, patient with PH, and patient treated with milrinone were normalized by their respective baseline results, which are hemodynamics of the Norwood patient without a pump. Table 1 shows the baseline results for an average Norwood patient.^{11,13} Table A1 presents baselines for a patient with PH and a patient treated with milrinone.

3.1 | Norwood patient

3.1.1 | Device volume

We simulated the BH at a device rate of 85 ppm, drive pressures of 220/−30 mm Hg, inflow connection at the atrium or the ventricular apex, and volumes of 10, 15, or 25 mL. While the ventricular BH had negligible effect on $Q_p:Q_s$, the 25 mL atrial BH reduced $Q_p:Q_s$ the most at 9.0%. As device volume increased, systemic oxygen delivery increased for both inflow connections due to increased cardiac output (Figure 2). However, there was no significant increase in SpO_2 (80.7% to 81.3% increase from baseline with increasing volume from 10 to 25 mL in a ventricular device; 81.4% to 83.4% increase with increasing volume in an atrial device). These results suggested that higher BH output from a larger device, not oxygen concentrations, drove the increase in delivery. However, independent of size, device implantation greatly improved oxygen delivery.

Increasing ventricular BH volume raised systolic pressures on average by 5.3%, 10.1%, and 15.9%, and decreased diastolic pressure by 4.5%, 6.7%, and 11.8% with a 10, 15, and 25 mL device, respectively. By contrast, increasing atrial BH volume increased both systolic pressure by 5.6%, 12.1%, and 16.4% and diastolic pressure by 0.5%, 5.0%, and 4.7% for the 10, 15, and 25 mL device, respectively. Interestingly, mean pulmonary arterial pressure (PAP)

decreased across both connections. However, SV–BH interactions caused a wide range of PAP (Figure A1).

As device volume increased, total CO and BH CO increased across both inflow connections. With a ventricular BH, total output increased by 43.8%, 45.8%, and 47.2% with a 10, 15, and 25 mL device, respectively. With the BH connected at the atrium, total CO increased by 48.4%, 55.6%, and 60.9% with a 10, 15, and 25 mL device, respectively. Although total CO increased more with an atrial BH, the ventricular BH operates with higher stroke volume and output. Moreover, given a theoretical output of 0.85, 1.28, and 2.13 L/min for a 10, 15, and 25 mL device, respectively, the ventricular BH operated at a higher efficiency than the atrial device—with efficiencies of 68.5%, 81.6%, and 73.4% for the 10, 15, and 25 mL ventricular device versus efficiencies of 45.4%, 28.0%, and 51.2% in the 10, 15, and 25 mL atrial devices. Total CO was higher with an atrial device because of greater SV CO. Relative to a patient without device implantation, the SV supplied 11.1% more output with a 10 mL atrial BH than a ventricular BH, 23.2% with a 15 mL atrial BH versus ventricular, and 34.9% more with a 25 mL atrial BH. These differences in SV CO were also reflected by trends in VSW.

With increasing device volume, VSW decreased across both inflow connections. However, the ventricular BH offloaded the SV by 2.5%–6.3% more. The ventricular BH reduced VSW more across all device volumes by offloading myocardial stress throughout the entire cardiac

TABLE 1 Comparison between clinical cohort of Norwood patients and baseline model.^{11,13}

Parameter	Clinical measurement	Tuned simulation result	%Error
CO (L/min)	2.04 ± 0.56	2.01	1.47%
Q_p (L/min)	1.07 ± 0.37	1.09	1.87%
Q_s (L/min)	0.96 ± 0.27	0.92	−4.17%
$Q_p:Q_s$	1.17 ± 0.40	1.18	0.85%
Sat _{art}	72.8% ± 4.9	76.1%	4.53%
Sat _{ven}	48.1% ± 5.6	50.2%	4.37%
Sys O ₂ delivery (mL/min)	156.84 ± 45.41	155.06	−1.13%
ΔAVO_2 (mL/dL)	N/A	5.73	N/A
SpO ₂ (mL/dL)	N/A	10.11	N/A
EDV (mL)	31.0 ± 3	30.78	−0.71%
ESV (mL)	14.0 ± 3	13.77	−1.64%
BP (mm Hg)	104 ± 14/45 ± 6	97/39	6.7%/13.3%
PAP (mm Hg)	13 ± 3	17.3	33.1%
VSW (mm Hg*mL)	N/A	1348.59	N/A

Note: Results are presented from simulations with tuned parameters to match clinical data.

Abbreviations: ΔAVO_2 , arteriovenous oxygen content difference; BP, blood pressure; EDV, end-diastolic volume; ESV, end-systolic volume; PAP, mean pulmonary arterial pressure; Q_p , pulmonary flow; Q_s , systemic flow; $Q_p:Q_s$, the ratio of pulmonary to systemic flow; Sat_{art}, arterial oxygen saturation; Sat_{ven}, venous oxygen saturation; SpO₂, arterial oxygen content; sys O₂ delivery, systemic oxygen delivery; VSW, ventricular stroke work.

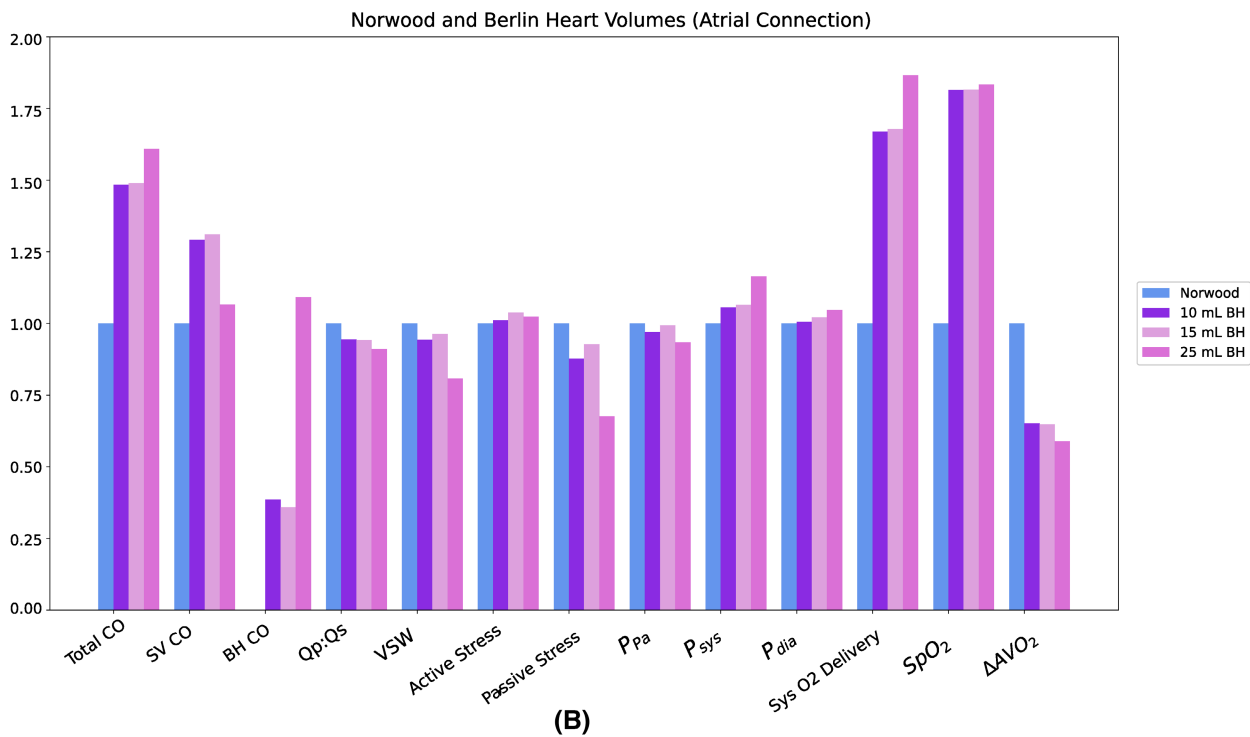
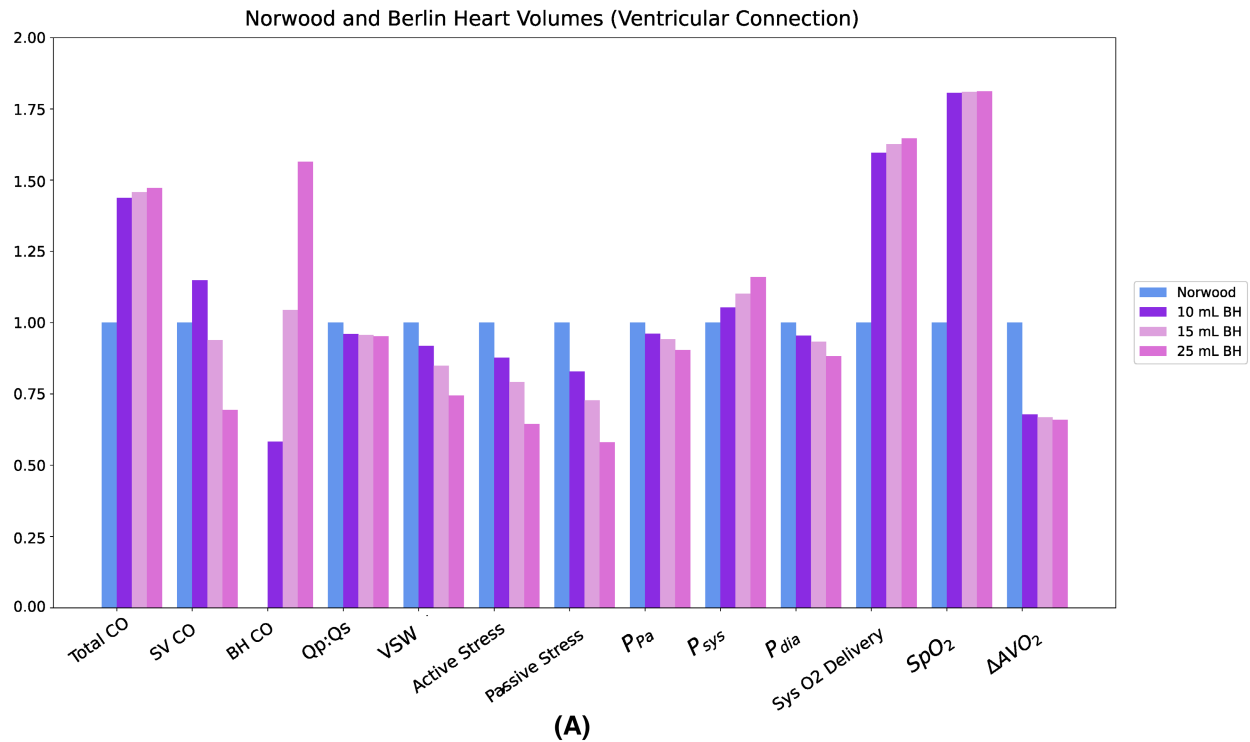


FIGURE 2 Normalized mean hemodynamic outcomes for a Norwood patient before BH implantation (blue) and after device implantation for volumes of 10 (purple), 15 (light pink), and 25 mL (fuchsia) with inflow connection at the (A) ventricular apex and (B) atrium. The raw values for BH CO are presented, as normalization by Norwood output would diminish the differences in output between device volumes. All other findings are normalized by baseline hemodynamic results of a Norwood patient without BH implantation.

cycle. At phases when SV systole coincided with ventricular BH filling, the SV pumped into the BH, which had a lower pressure than the ascending aorta, thus decreasing

afterload and VSW. When SV diastole coincided with ventricular BH filling, a synergistic decrease in pressure facilitated SV filling and offloaded the myocardium.



However, cycle-to-cycle variability in SV–BH interactions caused both cardiac offloading and overloading as the SV and BH oscillated between favorable and unfavorable phases (Figure A1). By contrast, myocardial active stress increased with the atrial BH due to SV–BH interactions; when SV systole coincides with BH ejection, the ventricle must pump against a higher afterload (Figure A2). The atrial BH decreased myocardial passive stress as it shunted preload to the BH instead of the SV. However, there was consistent offloading with the atrial BH as the device does not directly interact with the SV (Figure A1).

3.1.2 | Device rate

A 10 mL BH was simulated with drive pressures of 220/−30 mm Hg, inflow connections at the ventricular apex or atrium, and device rates of [60, 120], inclusive, at intervals of 10 ppm. Increasing BH rate decreased SV CO while increasing device output across both inflow connections (Figure 3A,B). Consistent with previous findings, the SV supplied 10.9% to 16.0% less output with a ventricular BH than atrial. The ventricular device provided 53.3% to 85.7% more output than the atrial. Overall, total CO did not vary significantly between device rates or connections. As SV CO decreased, increasing device output maintained total CO. In both devices, greater flow from the BH drove systemic oxygen delivery up, but with no substantial changes in SpO₂.

Both inflow connections results in cardiac offloading on average (6.8% to 9.6% reduction with a ventricular BH; 2.3% to 5.6% reduction with an atrial BH). The narrow range of SV CO suggested that variations in ventricular pressure caused the range of VSW. The ventricular BH reduced VSW by a greater extent on average, but produced oscillations between cardiac loading and overloading (Figure 3C). The ventricular device offloaded myocardial active and passive stress, whereas the atrial BH reduced only passive stress (Figure A2).

3.2 | Norwood patient with pulmonary hypertension

3.2.1 | Device volume

Increasing BH volume in a patient with PH displayed similar trends in total CO, SV CO, $Q_p:Q_s$, and SpO₂. Although SV CO decreased with increasing volume, its contribution only fell below baseline values with the ventricular BH at larger volumes (−7.9% and −33.7% with a 15 and 25 mL device, respectively). Increasing atrial BH volume reduced $Q_p:Q_s$, whereas a ventricular device had little effect. Our results showed that Norwood patients with PH require larger devices to pump against higher vascular resistances and achieve comparable reductions in SV CO and $Q_p:Q_s$ compared with those without (Figure 4). SpO₂ did not increase significantly with larger volumes (42.2% to 42.6% increase from baseline with a ventricular BH; 42.0% to 45.2% for an atrial BH). These findings supported that changing device volume may not affect systemic oxygen concentrations.

Results for VSW were consistent with previous findings that the ventricular BH reduced VSW more than the atrial BH (Figure A3). Similar SV–BH interactions to those described in Section 3.1 also governed VSW. The atrial BH decreased myocardial passive stress by lowering preload, whereas the ventricular BH reduced active and passive stress, offloading the SV to a greater extent overall (Figure A3). Decreased variability in cardiac loading was observed with the atrial BH across all device volumes.

Increasing ventricular BH volume reduced PAP by 2.0%, 2.8%, and 4.9% with a 10, 15, and 25 mL device, respectively (Figure A3). Systolic pressure increased by 5.3%, 10.1%, and 15.8% for a 10, 15, and 25 mL device, respectively. For an atrial BH, increasing volume raised systolic pressure up to 19.2%, diastolic pressure up to 10.8%, and PAP up to 4.0% (Figure A3). Both atrial and ventricular BH implantation resulted in extremes of PAP. Most notably, for both ventricular and atrial connections, the maximum PAP is greater

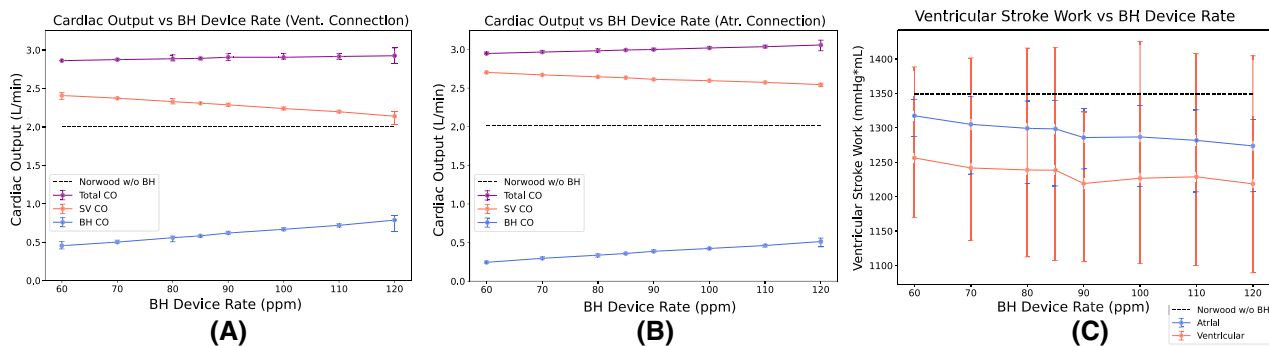


FIGURE 3 BH device rate versus (A) total CO (purple), SV CO (red), and BH CO (blue) for a ventricular BH, (B) total CO (purple), SV CO (red), and BH CO (blue) for an atrial BH, and (C) VSW for ventricular and atrial devices. Ranges for each metric are indicated by bars to reflect phase shifts (from $-\pi$ to π) and variations in SV–BH interactions.

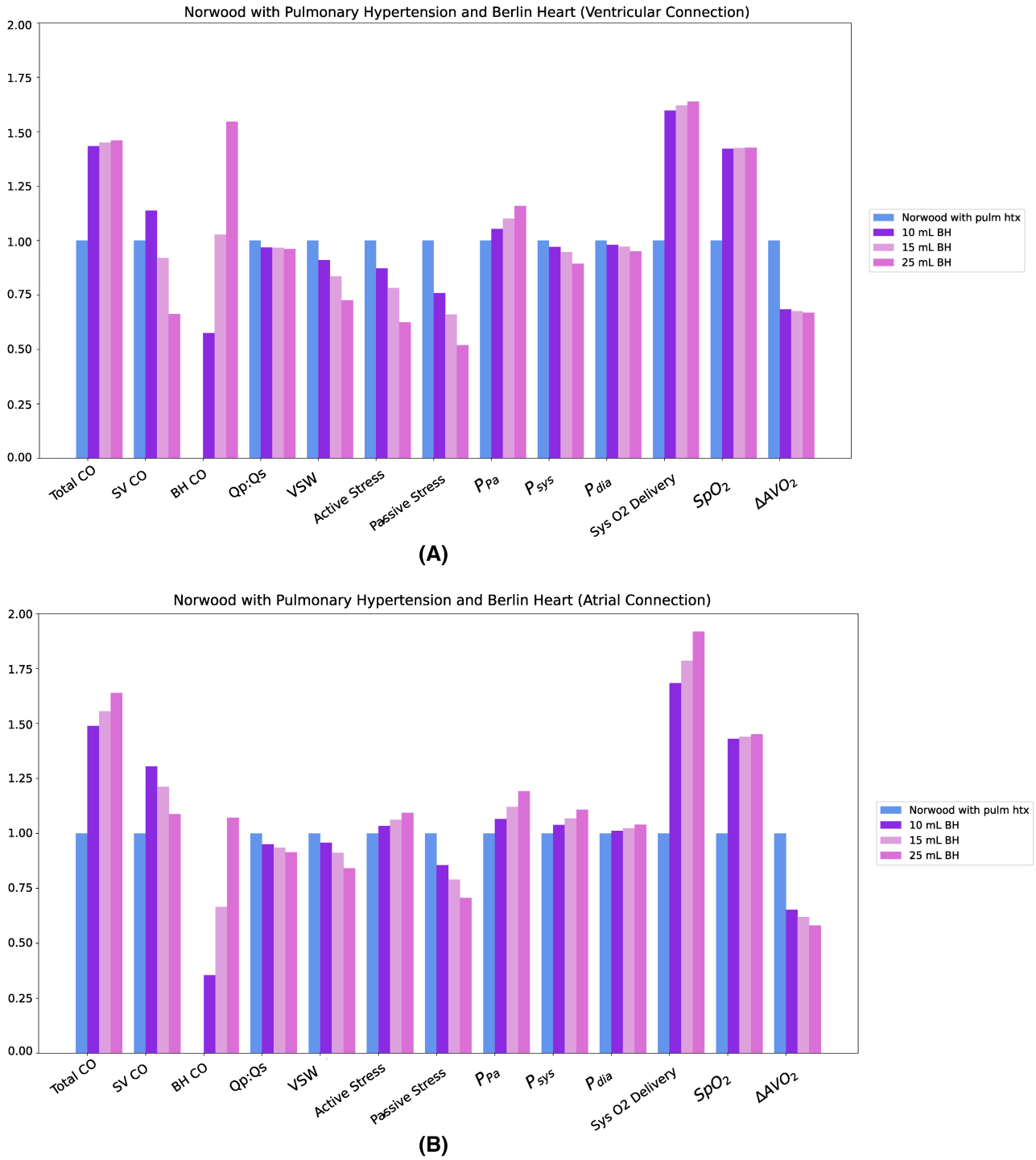


FIGURE 4 Normalized mean hemodynamic outcomes for a Norwood patient with PH before BH implantation (blue) and after device implantation for volumes of 10 (purple), 15 (light pink), and 25 mL (fuschia) with inflow connections at the (A) ventricular apex and (B) atrium. The raw values for BH CO are presented, as normalization by Norwood output would diminish the differences in output between device volumes. All other findings are normalized by baseline hemodynamic results of a Norwood patient without BH implantation.

at all pump volumes than without BH implantation. These extrema in PAP occurred due to unfavorable phase shifts between the SV and BH. Our findings demonstrated that Norwood patients with PH may be more vulnerable to extreme blood pressures when upsizing the BH.

3.2.2 | Device rate

As device rate increased, SpO₂ did not increase significantly (41.9% to 42.5% for a ventricular BH; 42.5% to 43.5% for an atrial BH); however, device implantation improved

oxygen circulation over baseline measurements, independent of rate. $Q_p:Q_s$ did not vary significantly from baseline values with increasing device rate. Overall CO increased slightly as the BH contributed more output to compensate for decreasing SV CO (Figure 5). This trend supported previous results in Section 3.2. However, the ventricular BH affected SV contribution more than the atrial BH, suggesting that patients with PH may be more sensitive to inflow connection. The narrow range of SV CO across both connections further demonstrated that oscillations between cardiac offloading and overloading were driven by changes in ventricular pressures.

With increasing rate in both atrial and ventricular BHs, passive stress in the myocardium decreased (Figure A4). While the atrial BH increased active stress in the myocardium for all device rates, the ventricular BH decreased active stress, which may be beneficial for patients with PH or with an overloaded SV. Device rate and cardiac offloading varied nonlinearly, emphasizing the effects of phase and SV–BH interactions, in addition to the importance of selecting an appropriate device rate.

3.3 | Norwood patient with milrinone

3.3.1 | Device volume

As BH volume increased, systemic oxygen delivery increased without significant changes to SpO_2 at any device size—in contrast to previous findings in Sections 3.1 and 3.2, where BH implantation increased SpO_2 . However, taken together, these findings consistently supported that higher BH output drove increases in delivery without improving oxygen concentration. Similar trends in SV CO and BH CO were also observed (Figure 6). For a ventricular BH, SV CO increased by 18.0% with a 10 mL device but decreased slightly with the 15 and 25 mL BHs. With an atrial BH, SV CO increased by 33.5%, 26.7%, and 19.9% for

a 10, 15, and 25 mL device, respectively. Consistent with previous results, the ventricular BH supplied more output. There were no significant changes in systolic pressure. Increasing device volume decreased diastolic pressure by up to 24.0% with a ventricular BH and up to 8.4% with an atrial BH. Similarly, PAP decreased up to 22.4% with a ventricular BH and up to 16.0% with an atrial BH. Device support complemented the vasodilating properties of milrinone, which decreases PVR. No significant changes in $Q_p:Q_s$ were observed with increasing device volume for the ventricular and atrial BHs.

VSW, active stress, and passive stress decreased nonlinearly with ventricular BH volume (Figures A5 and A6). Device implantation countered the therapeutic effects of milrinone, which increases ventricular contractility. With an atrial BH, VSW increased by 9.3% and 6.6% with the 10 and 15 mL devices, respectively. However, VSW decreased by 8.1% for a 25 mL atrial BH. Although myocardial active and passive stress increased, VSW decreased because of lower SV output and higher BH output. The atrial BH was synergistic with milrinone by increasing myocardial stress and thus, ventricular contractility. Our findings quantified the relationship between BH configurations, milrinone infusion, and SV contractility.

3.3.2 | Device rate

Across all device rates, the ventricular and atrial devices increased total CO by comparable magnitude (41.9% to 45.5% with a ventricular BH; 47.0% to 52.3% with an atrial BH). Consistent with previous results, increasing BH rate in a Norwood patient with milrinone in turn decreased SV contribution (−22.2% to −12.0% for a ventricular BH; −35.8% to −30.2%; Figure 7). While SV CO was greater than the baseline at all device rates, this was likely due to milrinone increasing ventricular contractility. At all device rates, the ventricular BH provided more output than

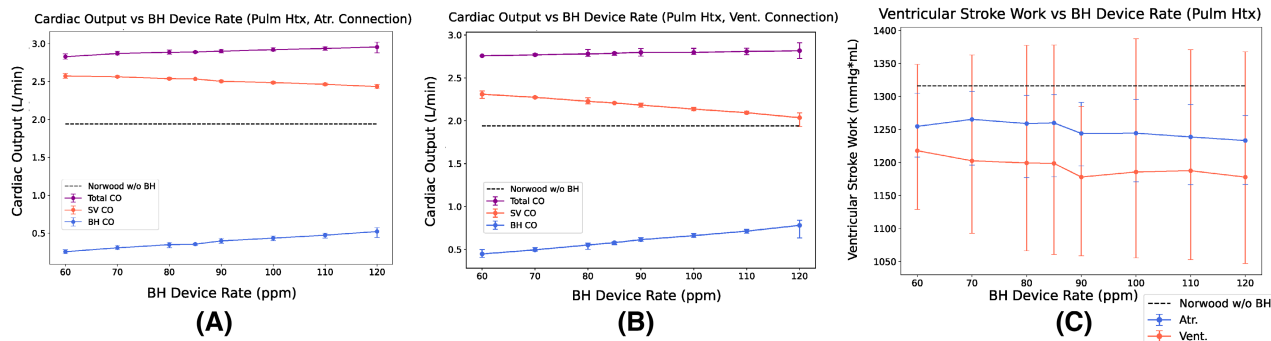


FIGURE 5 BH device rate versus (A) total CO (purple), SV CO (red), and BH CO (blue) for a ventricular BH, (B) total CO (purple), SV CO (red), and BH CO (blue) for an atrial BH, and (C) VSW for ventricular and atrial devices in a Norwood patient with PH. Ranges for each metric are indicated by bars to reflect variations in SV–BH interactions.

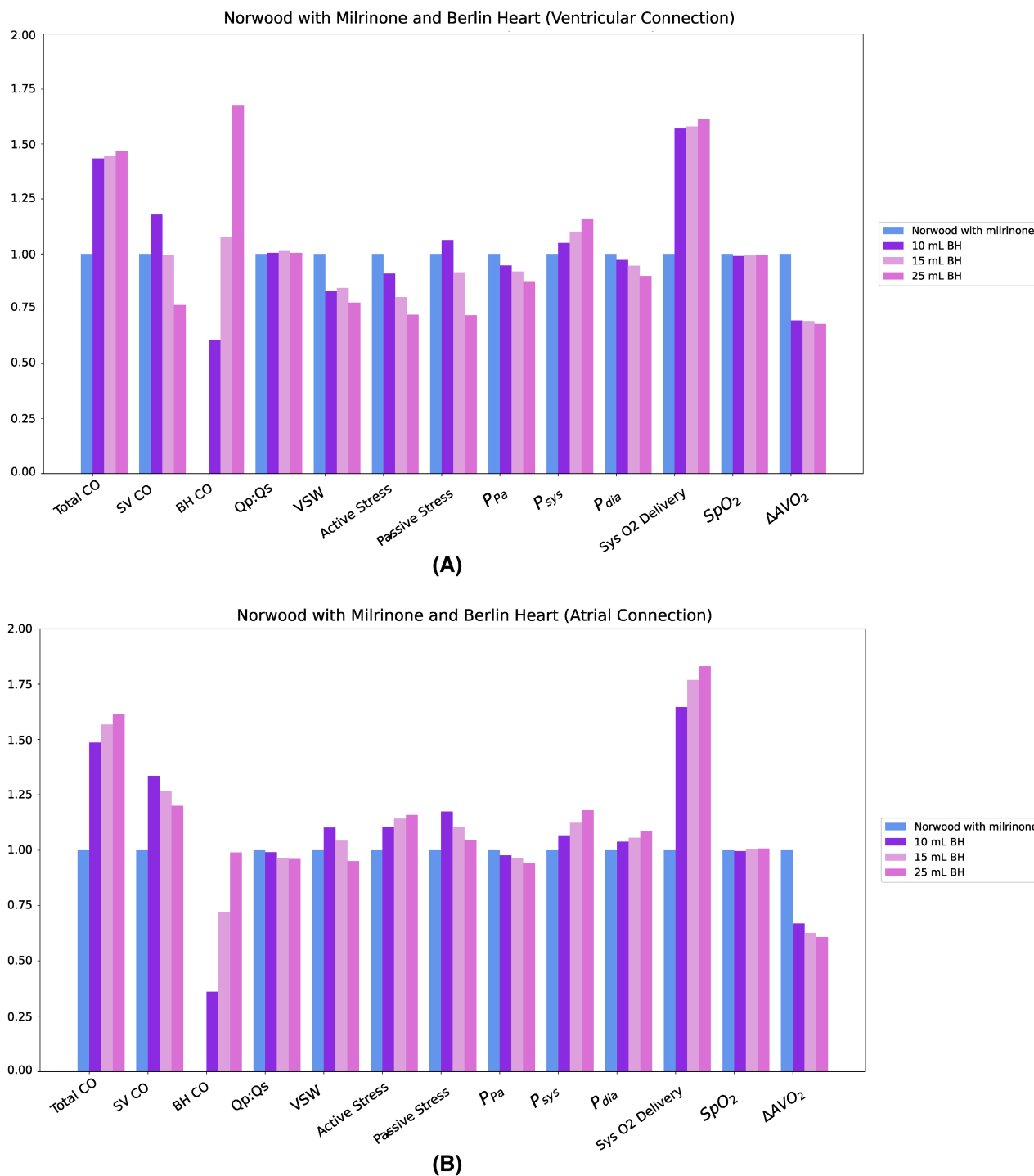


FIGURE 6 Normalized mean hemodynamic outcomes for a Norwood patient with milrinone treatment before BH implantation (blue) and after device implantation for volumes of 10 (purple), 15 (light pink), and 25 mL (fuschia) with inflow connections at the (A) ventricular apex and (B) atrium. The raw values for BH CO are presented, as normalization by Norwood output would diminish the differences in output between device volumes. All other findings are normalized by baseline hemodynamic results of a Norwood patient without BH implantation.

the atrial BH, consistent with previous results. At higher rates, more flow from the ventricular and atrial BHs drove systemic oxygen delivery upward. No significant changes in SpO_2 or $Q_p:Q_s$ were observed for both connections across all device rates. In contrast to trends observed in

Sections 3.2 and 3.3, implanting the BH with either connection did not offload the native SV.

The 10 mL atrial BH resulted in cardiac overloading at all device rates (VSW increased by 7.5%–9.2%; Figure A6). Myocardial active and passive stress

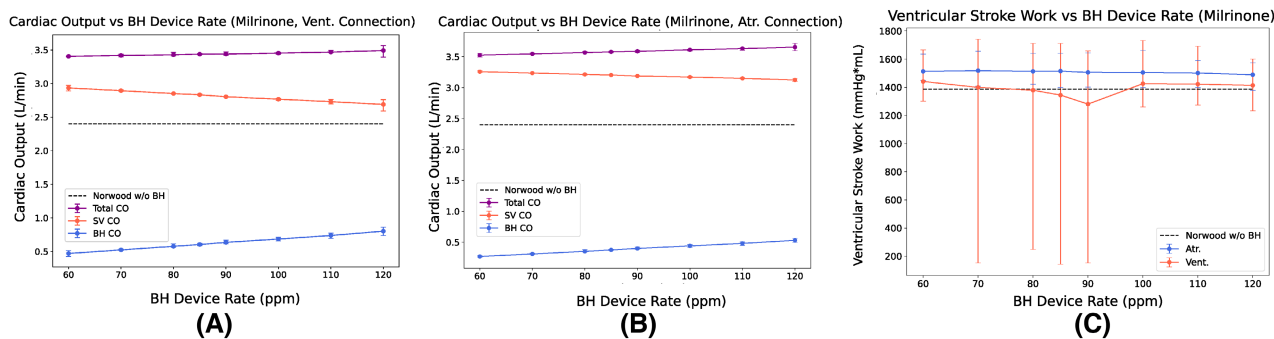


FIGURE 7 BH device rate versus (A) total CO (purple), SV CO (red), and BH CO (blue) for a ventricular BH, (B) total CO (purple), SV CO (red), and BH CO (blue) for an atrial BH, and (C) VSW for ventricular and atrial devices in a Norwood patient treated with milrinone. Ranges for each metric are indicated by bars to reflect variations in SV–BH interactions.

increased for all rates with the atrial device, indicating greater SV contractility and synergy with the inotropic effects of milrinone (Figure A6). For all device rates, the ventricular BH increased passive stress and reduced active stress compared with baseline values. The negative derivative of myocardial stress with respect to device rate in a ventricular BH suggested that higher rates may increasingly lower myocardial stress and oppose milrinone. Additionally, the ventricular BH offloaded the SV at 85 and 90 ppm, where SV–BH interactions favored extreme offloading and reduced VSW on average (Figure 7). Patients with milrinone infusions may be more sensitive to modulating device rate, which can impact SV–BH interactions that in turn govern ventricular loading.

4 | DISCUSSION

Placing the BH in Norwood patients has shown improvements in post-operative outcomes and survival. However, the relationship between patient hemodynamics and device size, rate, and inflow connection is not thoroughly characterized. This in turn makes it difficult to determine appropriate device configurations.^{3,5} Computational modeling can clarify interactions between the BH and native circulation for a wide range of clinical scenarios and inform decision-making on treatments.

To this end, we developed a mechanical–physiologic lumped model of a Norwood patient to analyze the cellular and organ-level outcomes of modulating BH volume, rate, and inflow connection across three different clinical scenarios. While previous models explored continuous VADs in SV physiology and did not change device settings, our study simulated a pulsatile VAD and its performance over different device configurations, which is more clinically realistic.¹⁹ We demonstrated that our model can be readily adjusted to analyze diverse clinical scenarios, from various

patient physiologies to post-operative therapies. By quantifying changes in pressures, VSW, and oxygen saturation after BH implantation, we painted a fuller picture of device support and suggest explanations for poor performance and mixed clinical outcomes. Additionally, our model examines bulk myocardial dynamics and offers a mechanistic understanding of cardiac unloading, which was lacking in prior models.^{11,13,19,21} Our findings emphasized how device parameters may be modulated to achieve post-operative targets and balance hemodynamic outcomes in patients with varied pathophysiologies and treatments.

First, across all device rates and volumes for all patient scenarios, device support reached clinical targets of $Q_p:Q_s < 1$.^{26,31} In patients with and without PH, SpO_2 increased significantly for ventricular and atrial BHs. However, increased device rate and volume did not raise SpO_2 , suggesting that oxygen concentration is independent of BH output. These results emphasize that despite increasing device support, oxygen delivery does not rise as expected. This phenomenon may contribute to suboptimal clinical outcomes in Norwood patients as the BH may not adequately meet their oxygen needs.

Secondly, our study investigated the mechanisms of BH support in Norwood patients with PH ($PVR = 7.0$ WU) and suggests that a BH with a larger volume and ventricular connection may be more appropriate for these patients. Increasing the volume of a ventricular BH increased CO and SpO_2 while offloading the native SV (Figure 4); however, this may come at the expense of increasing systolic pressure. Overall, these findings may explain clinical observations of significantly improved outcomes in patients with mechanical circulatory support and $PVR > 6$ WU.³² An atrial BH, on the contrary, caused extreme pulmonary arterial, systolic, and diastolic pressures. These findings emphasize that an atrial BH may be inappropriate for Norwood patients with PH by straining the SV. Specifically, increased pulmonary arterial pressure in these patients may exacerbate PH, which may increase



risk for complications such as cardiac arrest.⁶ Increased pressures were also observed in Norwood patients without PH. Similarly, these extreme pressures may limit the benefits of VAD support, offering a rationale for mixed clinical outcomes. However, our studies suggested that coupling device support with milrinone may mitigate increased pressures. With a 25 mL ventricular BH, a Norwood patient without milrinone has a PAP of 16 mm Hg and blood pressure (BP) 112/34 versus a patient with milrinone with a PAP of 13 mm Hg and BP 106/30 (Figures A1 and A5). Our model can help investigate the balance between CO, pressures, BH configurations, and the regulatory effect of post-operative therapies on this relationship. While our study simulated only milrinone, we demonstrated how experimental studies and clinical measurements can be integrated into our model to explore different pharmaceuticals.

Third, studying BH support and settings in our model revealed insights about myocardial stress and SV–BH interactions that impact VSW. The ventricular BH decreased active and passive stress in the myocardium while maintaining total CO. Myocardial passive stress decreased as BH filling due to negative drive pressure in turn facilitated ventricular diastole. Active stress was reduced when the SV ejected into the BH, which had lower pressure than the aorta, thus decreasing SV peak pressure. Such unloading may benefit myocardial structure.³³ In particular, the atrial BH offloaded the SV throughout the entire cardiac cycle with less variability. Such consistencies may be especially beneficial for patients with diastolic dysfunction. However, the atrial BH amplified myocardial active stress, which may be of concern for stressed hearts. The ventricular BH oscillated between offloading and overloading, which may negatively affect cardiac remodeling and thus patient health. In particular, inconsistent cardiac loading may worsen clinical outcomes in Norwood patients with diastolic dysfunction. The ventricular BH also countered milrinone by decreasing myocardial stress, particularly at rates of 85 and 90 ppm. These results suggested that a greater concentration of milrinone may be necessary when coupled with a ventricular device. In contrast, the atrial BH and milrinone had a synergistic effect on ventricular contractility. Further studies are necessary to explore clinical scenarios where BH support and pharmaceuticals are coupled. Our simulation highlighted variability in cardiac loading and myocardial stress due to BH connection and rate. These insights may guide device settings for patients with diverse etiologies and needs.

4.1 | Limitations and future work

One limitation of our methodology is shortened simulation time. When the BH operated at 85bpm and the SV

at 120bpm, simulation results were averaged over 9 s. However, a simulation of 12 s should be performed to model the full-phase interaction and obtain an integer number of cycles for both the SV and BH; this consists of 24 cycles for the SV and 17 cycles for the BH. Although we averaged results over 9 s for each simulation, our methodology modeled 9 different phase shift shifts from $[-\pi, \pi]$ of SV–BH interactions; thus for each SV–BH rate combination, the total simulation time was 81 s. This approach allowed us to thoroughly capture the full-phase interaction between SV and BH, despite the shortened simulation time. When the SV and BH pump at different rates, they also move through different phase shifts in the interval $[-\pi, \pi]$. For example, at a phase shift of 0, the SV and BH will also vary at phase shifts of $-\pi, -3\pi/4, -\pi/2, \dots, \pi$. A simulation of phase shift = 0 and phase shift = $\pi/2$ shared a high fraction of its SV–BH interactions (Figure A7). Thus, explicitly simulating different phase shifts for a given SV–BH rate combination can capture the full range of interactions that would otherwise be observed with a longer simulation time. To this end, we also performed simulations with the SV at 120bpm and the BH at 85 ppm for phase shifts of 0, $\pi/2$, and π while extending simulation time by 3 s to capture the full-phase interaction. We found that the difference in CO between the shorter and longer simulations was only 1%; this analysis demonstrates that given our methodology of modeling phase shifts, a longer simulation time is not likely to affect our results. However, future studies should simulate the full-phase interaction between the SV and BH.

Moreover, due to a lack of clinical data on Norwood patients before and after BH implantation, our results are not comprehensive. Rather, our study leverages existing and clinically validated *in silico* models.^{11,21,22} Moreover, it is not exhaustive in simulating pathological conditions or post-operative therapies. Future work could also include prospective collection of clinical data to produce more clinically realistic models, explore their predictive ability, and simulate other common pharmaceuticals such as vasopressin and romodulin.²⁷ Our study is also limited in spatial information. Future work could involve computational fluid dynamics with 3D geometries of the ascending aorta, pulmonary artery, and shunt to obtain a more localized understanding of hemodynamics. Further validation is needed in this younger patient population and under varying physiologic conditions. However, this is beyond the scope of our work, as we focus on the global hemodynamics of BH implantation in SV patients. Additionally, data to simulate myocardial dynamics after milrinone treatment was taken from canine experiments, limiting its applicability to human myocardium. To our knowledge, no such data with human tissue exist. Nevertheless, we demonstrated the utility of our model in capturing the effects of post-operative therapies.



5 | CONCLUSION

Single-ventricle Norwood patients face the worst outcomes of all infants and children on the Berlin Heart EXCOR (BH).⁴ Treatment for Norwood patients is impeded by an incomplete knowledge of how device settings impact the native circulations.^{3,5} With computational modeling, we quantified the impact of different BH volumes, rates, and inflow connections on cellular and tissue-level behavior in a Norwood patient. We investigated three clinical scenarios and demonstrated the flexibility of our model to explore diverse questions, such as coupling BH treatment with post-operative pharmacologics. We showed that increasing BH volume and rate can increase total CO, decrease VSW, and balance pulmonary and systemic flows. Though pressures increased, our simulations suggested that post-operative milrinone infusion may ameliorate these issues. SpO₂ was improved by device implantation, but it was independent of volume, rate, or connection. Our findings identified mechanisms of cardiac unloading and its relationship with BH settings. In particular, an atrial BH consistently offloaded the SV throughout the cardiac cycle, which may benefit patients with diastolic dysfunction; our results suggested that fitting Norwood patients with PH with a larger, ventricular BH may decrease myocardial active stress. Insights from computational modeling may assist clinicians in determining BH treatment and post-operative therapies for patients with distinct needs.

AUTHOR CONTRIBUTIONS


Conceptualization, V.Y., F.D.G., M.L.C.; Methodology, V.Y., F.D.G.; Data analysis, V.Y.; Statistics, V.Y.; Investigation, V.Y., M.L.C., A.L.M.; Funding secured by V.Y.; Writing - original draft, V.Y.; Writing - review and editing, V.Y., F.D.G., K.O., A.L.M., M.L.C.; Supervision, A.L.M., M.L.C.

CONFLICT OF INTEREST STATEMENT

The authors do not have any conflicts of interest to report.

ORCID

Victoria Yuan  <https://orcid.org/0000-0002-9411-5233>

Francesco De Gaetano  <https://orcid.org/0000-0002-7597-020X>

Maria Laura Costantino  <https://orcid.org/0000-0001-6974-2692>

REFERENCES

1. Gaynor JW, Mahle WT, Cohen MI, Ittenbach RF, DeCampi WM, Steven JM, et al. Risk factors for mortality after the Norwood procedure. *Eur J Cardiothorac Surg.* 2002;22:82–9.
2. Almond CS, Morales DL, Blackstone H, Turrentine MW, Imamura M, Massicotte MP, et al. Berlin Heart EXCOR pediatric ventricular assist device for bridge to heart transplantation in US children. *Circulation.* 2013;127:1711–20.
3. Gorbea M. A review of physiologic considerations and challenges in pediatric patients with failing single-ventricle physiology undergoing ventricular assist device placement. *J Cardiothorac Vasc Anesth.* 2022;36:1756–70.
4. Weinstein S, Bello R, Pizarro C, Fynn-Thompson F, Kirklin J, Guleserian K, et al. The use of the Berlin Heart EXCOR in patients with functional single ventricle. *J Thorac Cardiovasc Surg.* 2014;147:697–704.
5. Horne D, Conway J, Rebeyka IM, Buccholz H. Mechanical circulatory support in univentricular hearts: current management. *Semin Thorac Cardiovasc Surg Pediatr Card Surg Annu.* 2015;18:17–24.
6. Loomba RS, Rausa J, Farias JS, Villarreal EG, Acosta S, Savorgnan F, et al. Impact of medical interventions and comorbidities on Norwood admission for patients with hypoplastic left heart syndrome. *Pediatr Cardiol.* 2022;43:267–78.
7. Hornik CP, He X, Jacobs JP, Li JS, Jaquiss RDB, Jacobs ML, et al. Complications after the Norwood operation: an analysis of the STS congenital heart surgery database. *Ann Thorac Surg.* 2011;92:1734–40.
8. Mackling T, Shah T, Dimas V, Guleserian K, Sharma M, Forbess J, et al. Management of single-ventricle patients with Berlin Heart EXCOR ventricular assist device: single-center experience. *Artif Organs.* 2012;36:555–9.
9. Hetzer R, Kaufmann F, Delmo Walter EM. Paediatric mechanical circulatory support with Berlin Heart EXCOR: development and outcome of a 23-year experience. *Eur J Cardiothorac Surg.* 2016;50:203–10.
10. Giovanni B, Alessandro G, Baker C, Figliola RS, Hsia T-Y, Taylor AM, et al. In vitro study of the Norwood palliation a patient-specific mock circulatory system. *ASAIO J.* 2012;58:25–31.
11. Migliavacca F, Pennati G, Dubini G, Fumero R, Pietrabissa R, Urcelay G, et al. Modeling of the Norwood circulation: effects of shunt size, vascular resistances, and heart rate. *Am J Physiol Heart Circ Physiol.* 2001;280:H2076–86.
12. Hsia TY, Cosentino D, Corsini C, Pennati G, Dubini G, Migliavacca F, et al. Use of mathematical modeling to compare and predict hemodynamic effects between hybrid and surgical Norwood palliations for hypoplastic left heart syndrome. *Circulation.* 2011;124:S204–10.
13. Corsini C, Biglino G, Schievano S, Hsia TY, Migliavacca F, Pennati G, et al. The effect of modified Blalock-Taussig shunt size and coarctation severity on coronary perfusion after the Norwood operation. *Ann Thorac Surg.* 2014;98:648–54.
14. Moghadam ME, Migliavacca F, Vignon-Clementel IE, Hsia TY, Marsden AL, Modeling of Congenital Hearts Alliance (MOCHA) Investigators. Optimization of shunt placement for the Norwood surgery using multi-domain modeling. *J Biomech Eng.* 2012;134:051002.
15. Qian Y, Liu J, Itatani K, Miyaji K, Umezumi M. Computational hemodynamic analysis in congenital heart disease: simulation of the Norwood procedure. *Ann Biomed Eng.* 2010;38:2302–13.
16. Bhavsar SS, Kapadia JY, Chopski SG, Throckmorton AL. Intravascular mechanical cavopulmonary assistance for patients with failing Fontan physiology. *Artif Organs.* 2009;33:977–87.



17. Pekkan K, Frakes D, Zelicourt DD, Lucas CW, Parks WJ, Yoganathan AP. Coupling pediatric ventricle assist devices to the Fontan circulation: simulations with a lumped-parameter model. *ASAIO J*. 2005;51:618–28.
18. Nguyen T, Argueta-Morales IR, Guimond S, Clark W, Ceballos A, Osorio R, et al. Computational analysis of pediatric ventricular assist device implantation to decrease cerebral particulate embolization. *Comput Methods Biomech Biomed Engin*. 2016;19:789–99.
19. Di Molfetta A, Amodeo A, Gagliardi MG, Trivella MG, Fresiello L, Filippelli S, et al. Hemodynamic effects of ventricular assist device implantation on Norwood, Glenn, and Fontan circulations: a simulation study. *Artif Organs*. 2016;40:34–42.
20. Griselli M, Sinha R, Jang S, Perri G, Adachi I. Mechanical circulatory support for single ventricle failure. *Front Cardiovasc Med*. 2018;5:115.
21. Yuan V, Verma A, Schiavone NK, Rosenthal DN, Marsden AL. A mechanistic lumped parameter model of the Berlin Heart EXCOR to analyze device performance and physiologic interactions. *Cardiovasc Eng Technol*. 2022;13(4):603–23.
22. Pant S, Corsini C, Baker C, Hsia TY, Pennati G, Vignon-Clementel IE, et al. Data assimilation and modeling of patient-specific single-ventricle physiology with and without valve regurgitation. *J Biomech*. 2016;49:2162–73.
23. Mynard J, Davidson M, Penny D, Smolich J. A simple, versatile valve model for use in lumped parameter and one-dimensional cardiovascular models. *Int J Numer Method Biomed Eng*. 2012;28:626–41.
24. Feinstein JA, Benson DW, Dubin AM, Cohen MS, Maxey DM, Mahle WT, et al. Hypoplastic left heart syndrome: current considerations and expectations. *J Am Coll Cardiol*. 2012;59:S1–42.
25. Zuppa AF, Nicolson SC, Adamson PC, Wernovsky G, Mondick JT, Burnham N, et al. Population pharmacokinetics of milrinone in neonates with hypoplastic left heart syndrome undergoing stage I reconstruction. *Anesth Analg*. 2006;102:1062–9.
26. Hoffman GM, Tweddell JS, Ghanayem NS, Mussatto KA, Stuth EA, Jaquis RDB, et al. Alteration of the critical arteriovenous oxygen saturation relationship by sustained afterload reduction after the Norwood procedure. *J Thorac Cardiovasc Surg*. 2004;127:738–45.
27. Li J, Zhang G, Benson L, Holtby H, Cai S, Humpl T, et al. Comparison of the profiles of postoperative systemic hemodynamics and oxygen transport in neonates after the hybrid or the Norwood procedure: a pilot study. *Circulation*. 2007;116:1179–87.
28. Chang AC, Atz AM, Wernovsky G, Burke RP, Wessel DL. Milrinone: systemic and pulmonary hemodynamic effects in neonates after cardiac surgery. *Crit Care Med*. 1995;23:1907–14.
29. Gao B, Qu Y, Sutherland W, Chui RW, Hoagland K, Vargas HM. Decreased contractility and altered responses to inotropic agents in myocytes from tachypacing-induced heart failure canines. *J Pharmacol Toxicol Methods*. 2018;93:98–107.
30. GmbH BH. EXCOR pediatric VAD: ventricular assist device with stationary driving unit Ikus rev. 2.1, instructions for use 1000721x09 revision 8. 2015.
31. Tweddell JS, Hoffman GM, Fedderly RT, Ghanayem NS, Kampine JM, Berger S, et al. Patients at risk for low systemic oxygen delivery after the Norwood procedure. *Ann Thorac Surg*. 2000;69:1893–9.
32. Thangappan K, Morales D, Lehenbauer D, Lehenbauer D, Villa C, Wittekind S, et al. Impact of mechanical circulatory support on pediatric heart transplant candidates with elevated pulmonary vascular resistance. *J Heart Lung Transplant*. 2020;45(1):29–37.
33. Drakos SG, Kfoury AG, Selzman CH, Verma DR, Nanas JN, Li DY, et al. Left ventricular assist device unloading effects on myocardial structure and function: current status of the field and call for action. *Curr Opin Cardiol*. 2013;26:245–55.

How to cite this article: Yuan V, De Gaetano F, Osouli K, Marsden AL, Costantino ML. Investigating the hemodynamics of Berlin Heart EXCOR support in Norwood patients across diverse clinical scenarios with computational modeling. *Artif Organs*. 2023;00:1–18. <https://doi.org/10.1111/aor.14544>



APPENDIX A

Baseline

TABLE A1 Simulated hemodynamics for a Norwood patient with PH and a patient treated with milrinone.

Parameter	Patient with PH	Patient with milrinone treatment
CO (L/min)	1.94	2.40
Q_p (L/min)	0.99	1.02
Q_s (L/min)	0.95	1.38
$Q_p:Q_s$	1.04	0.74
Sat _{art}	74.0%	74.7%
Sat _{ven}	48.9%	57.4%
Sys O ₂ delivery (mL/min)	155.44	227.55
$\dot{V}AO_2$ (mL/dL)	12.60	18.28
SpO ₂ (mL/dL)	5.56	3.83
EDV (mL)	30.21	30.26
ESV (mL)	13.77	12.70
BP (mm Hg)	97/40	91/33
PAP (mm Hg)	25.9	15.3
VSW (mm Hg*mL)	1315.77	1385.67

Norwood patient

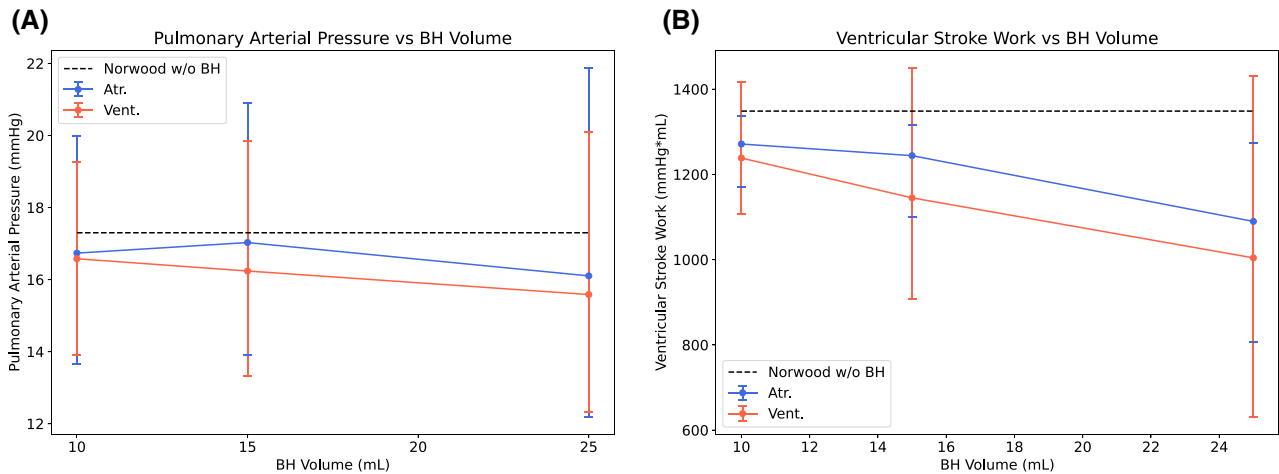


FIGURE A1 Mean, maximum, and minimum (A) mean pulmonary arterial pressure (B) mean VSW versus BH volume for the atrial BH (blue) and ventricular BH (red) and baseline values without device implantation in black.

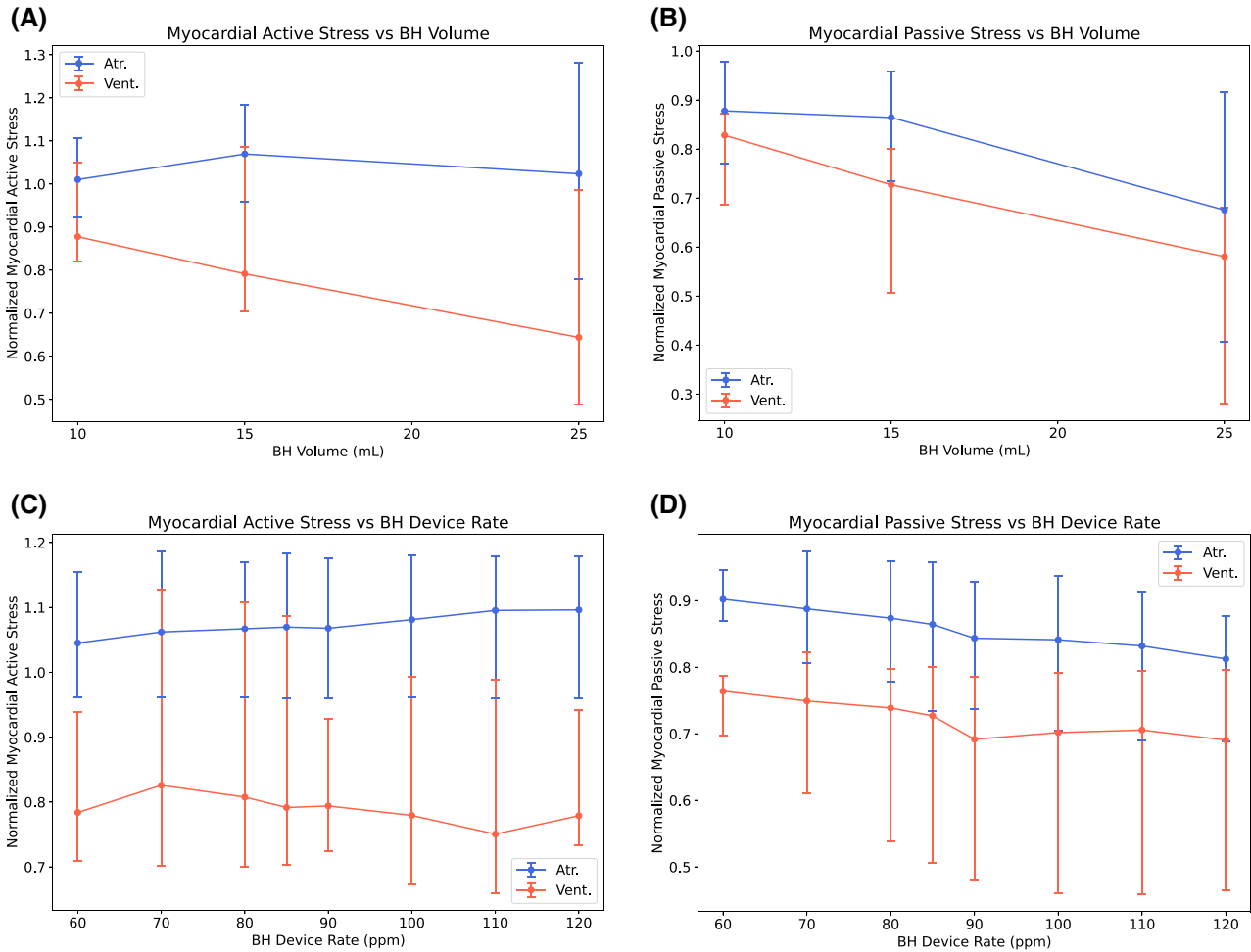


FIGURE A2 Normalized mean, maximum, and minimum myocardial active stress and passive myocardial stress versus (A, B) BH volume and (C, D) BH device rate.

Norwood patient with pulmonary hypertension

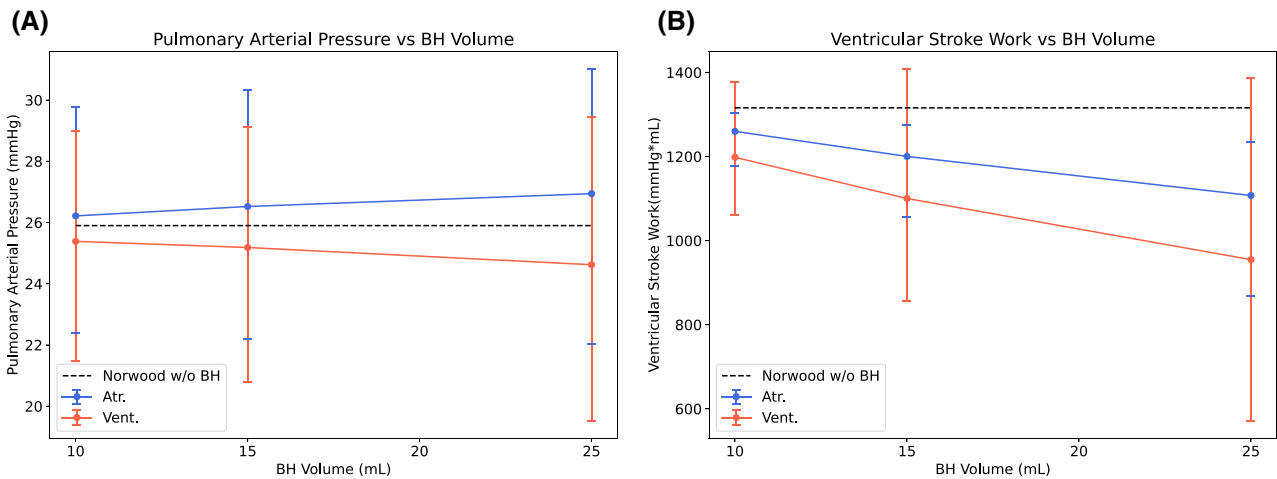


FIGURE A3 Mean, maximum, and minimum (A) mean pulmonary arterial pressure (B) mean VSW versus BH volume for the atrial BH (blue) and ventricular BH (red) and baseline values without device implantation in black in a Norwood patient with PH.

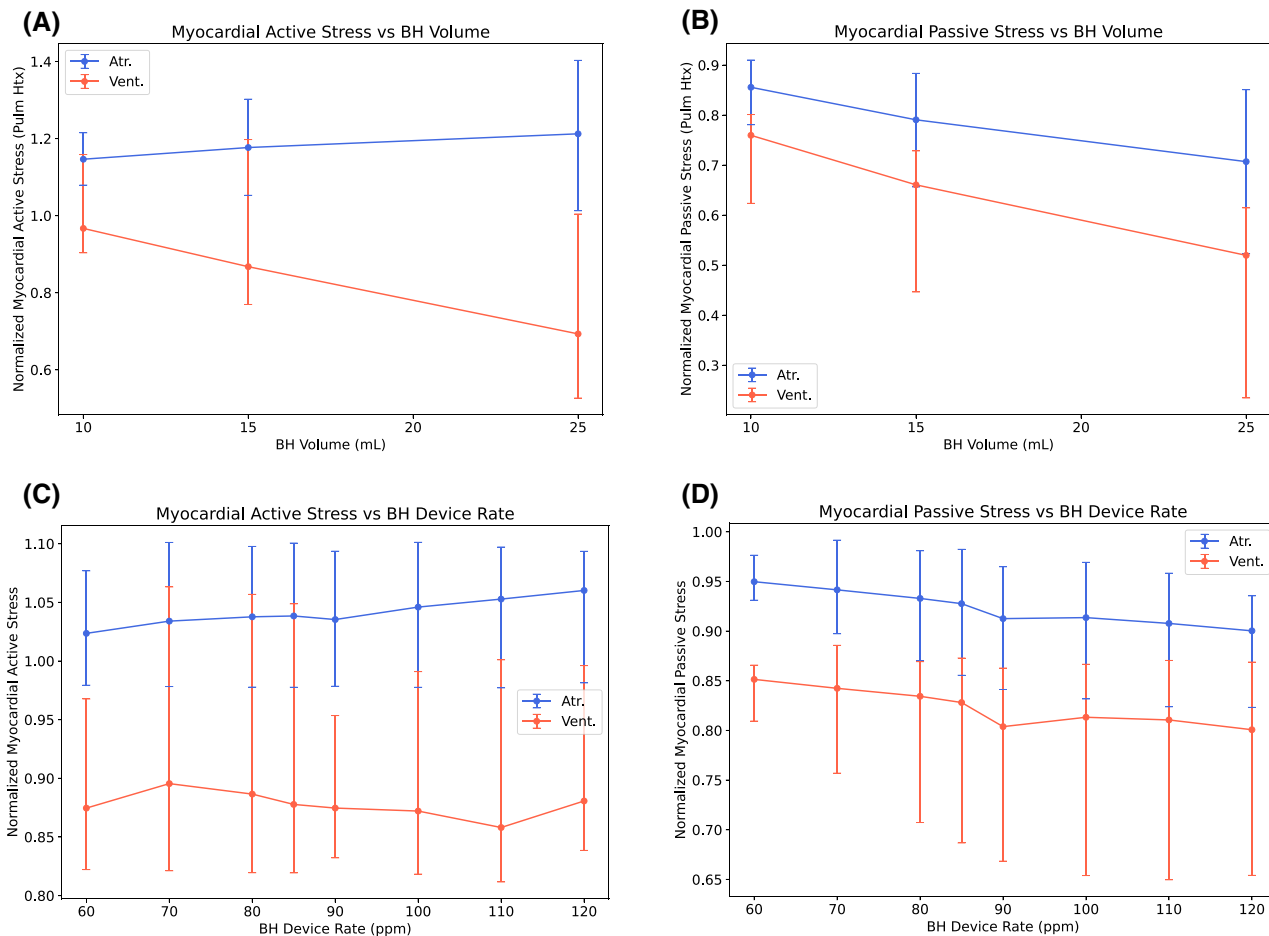


FIGURE A4 Normalized mean, maximum, and minimum myocardial active stress and passive myocardial stress versus (A, B) BH volume and (C, D) BH device rate in a patient with PH.

Norwood patient with milrinone infusion

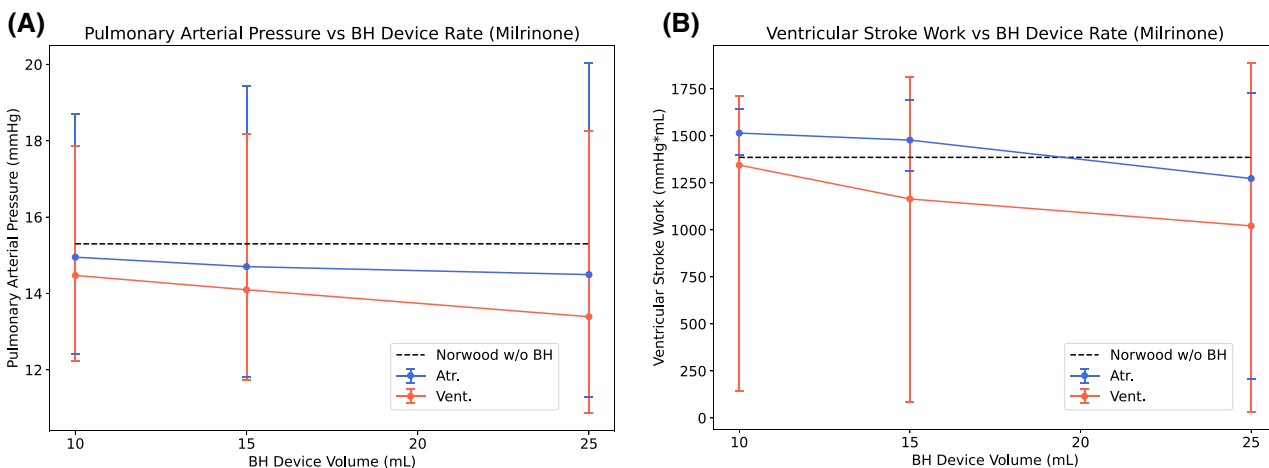


FIGURE A5 Mean, maximum, and minimum (A) mean pulmonary arterial pressure (B) mean VSW versus BH volume for the atrial BH (blue) and ventricular BH (red) and baseline values without device implantation in black in a Norwood patient treated with milrinone.

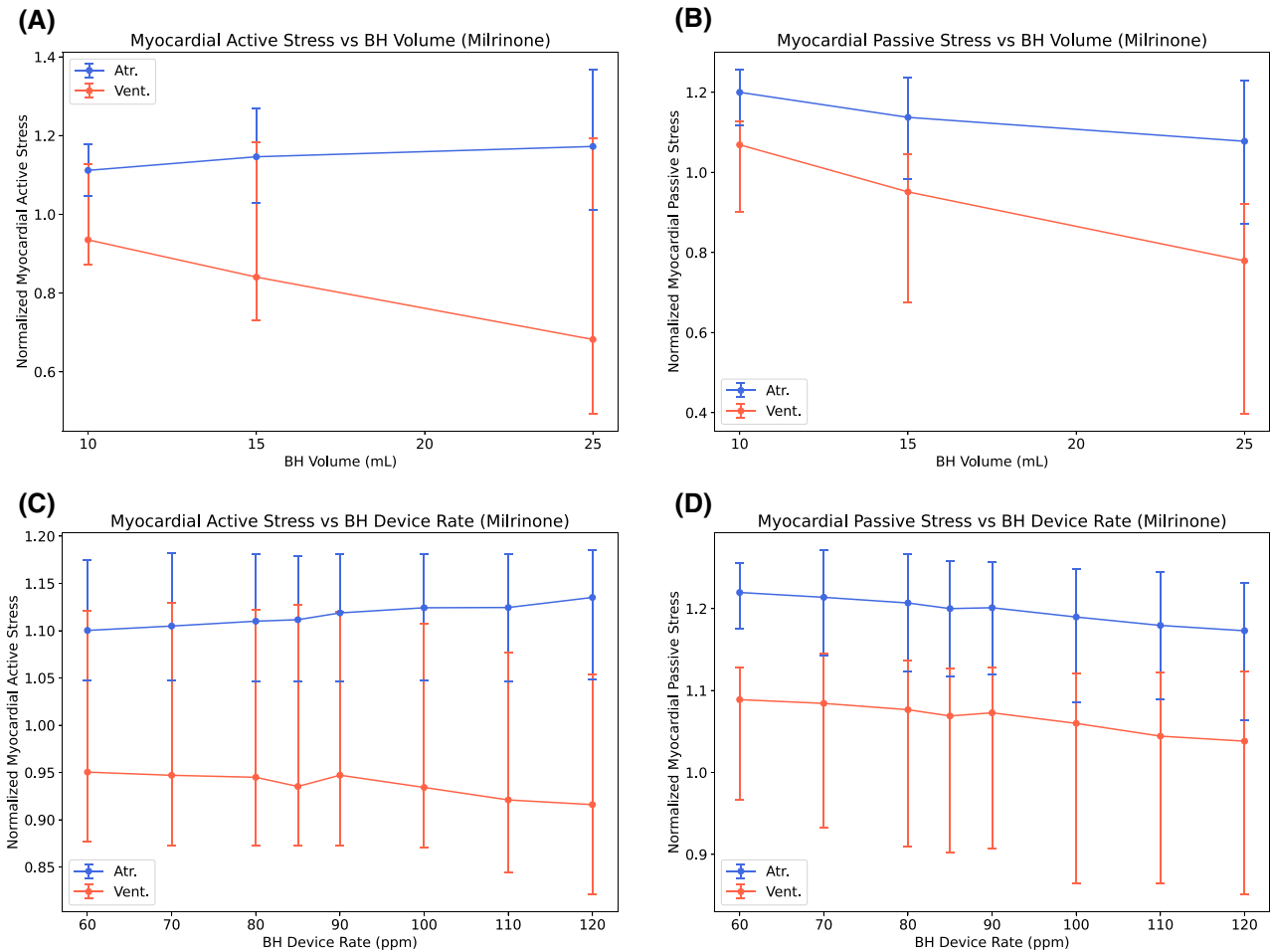


FIGURE A6 Normalized mean, maximum, and minimum myocardial active stress and passive myocardial stress versus (A, B) BH volume and (C, D) BH device rate in a patient treated with a standard milrinone infusion.

Phase shift analysis

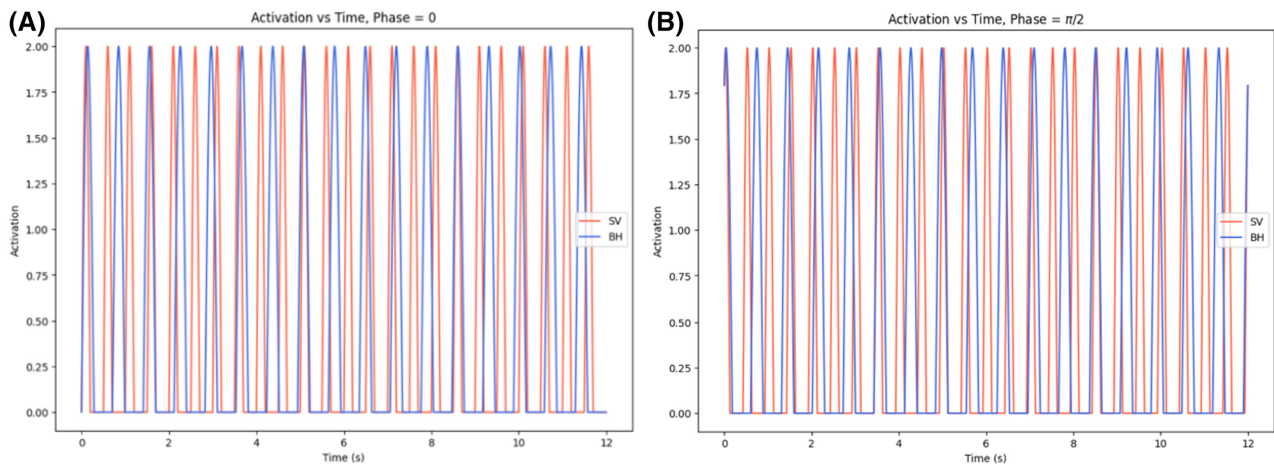


FIGURE A7 Activation functions of the SV pumping at 120 bpm (red) and BH operating at 85 ppm (blue) for (A) phase shift = 0 and (B) phase shift = $\pi/2$. The two-phase shifts share interactions such that averaging results across nine different phase shifts captures the full range of interactions that would otherwise be observed with a longer timescale.